Annales Geophysicae (2003) 21: 1017–1030 © European Geosciences Union 2003

Annales Geophysicae

Vertical $E \times B$ drift velocity variations and associated low-latitude ionospheric irregularities investigated with the TOPEX and GPS satellite data

I. Horvath and E. A. Essex

Department of Physics, La Trobe University Cooperative Research Centre for Satellite Systems, Bundoora, Victoria, 3086, Australia

Received: 4 February 2002 – Revised: 18 November 2002 – Accepted: 21 November 2002

Abstract. With a well-selected data set, the various events of the vertical $\boldsymbol{E} \times \boldsymbol{B}$ drift velocity variations at magnetic-equator-latitudes, the resultant ionospheric features at low- and mid-latitudes, and the practical consequences of these $\boldsymbol{E} \times \boldsymbol{B}$ events on the equatorial radio signal propagation are demonstrated. On a global scale, the development of a equatorial anomaly is illustrated with a series of 1995 global TOPEX TEC (total electron content) maps. Locally, in the Australian longitude region, some field-aligned TOPEX TEC cross sections are combined with the matching Guam (144.86° E; 13.59° N, geographic) GPS (Global Positioning System) TEC data, covering the northern crest of the equatorial anomaly. Together, the 1998 TOPEX and GPS TEC data are utilized to show the three main events of vertical $\boldsymbol{E} \times \boldsymbol{B}$ drift velocity variations: (1) the pre-reversal enhancement, (2) the reversal and (3) the downward maximum. Their effects on the dual-frequency GPS recordings are documented with the raw Guam GPS TEC data and with the filtered Guam GPS dTEC/min or 1-min GPS TEC data after Aarons et al. (1997). During these $\boldsymbol{E} \times \boldsymbol{B}$ drift velocity events, the Port Moresby (147.10° E; −9.40° N, geographic) virtual height or h'F ionosonde data (km), which cover the southern crest of the equatorial anomaly in the Australian longitude region, show the effects of plasma drift on the equatorial ionosphere. With the net (Δ) horizontal (H) magnetic field intensity parameter, introduced and called ΔH or $H_{equator}$-$H_{non-equator}$ (nT) by Chandra and Rastogi (1974), the daily $\boldsymbol{E} \times \boldsymbol{B}$ drift velocity variations are illustrated at 121° E (geographic) in the Australian longitude region. The results obtained with the various data show very clearly that the development of mid-latitude night-time TEC increases is triggered by the westward electric field as the appearance of such night-time TEC increases coincides with the $\boldsymbol{E} \times \boldsymbol{B}$ drift velocity reversal. An explanation is offered with the F-region dynamo theory and electrodynamics, and with the ionospheric-plasmaspheric coupling. A comparison is made with the published model results of SUPIM (Sheffield University Plasmasphere-Ionosphere Model; Balan and Bailey, 1995) and experimental results of Park (1971), and the good agreement found is highlighted.

Key words. Ionosphere (electric fields; equatorial ionosphere; mid-latitude ionosphere)

Correspondence to: I. Horvath
(I.Horvath@latrobe.edu.au)

1 Introduction

1.1 F-region dynamo and electrodynamics

In the ionospheric F-region (150–1000 km), the strong thermospheric neutral winds create vertically upward dynamo currents, which set up a vertical polarization field where the positive and negative charges accumulate at the top and bottom boundaries, respectively. During the daytime this polarization field becomes shorted out by the large conductivity of the sunlit E-layer (90–150 km). However, at nighttime, when the open circuit conditions apply, the winds maintain this polarization field. Hence, the positive and negative charges create an electric field (E) that interacts with the horizontal magnetic field (B) at and near the geomagnetic dip equator. The resultant drift velocity sets the ionospheric plasma into motion (Kelley, 1989):

$$\boldsymbol{v} = \frac{\boldsymbol{E} \times \boldsymbol{B}}{B^2} \,. \tag{1}$$

This electrodynamic lifting operates across the horizontal magnetic field lines at dip-equator-latitudes. It raises the low-latitude ionospheric plasma above the magnetic dip equator until the plasma becomes slowed down by the pressure forces. When the plasma loses momentum, it moves along the magnetic field lines under the forces of gravity and pressure gradients, and away from the magnetic equator. Finally, the plasma becomes deposited at higher dip-equator latitudes in both hemispheres. The combination of the upward plasma drift and downward diffusion along the magnetic field lines is called the plasma fountain effect, and the

resultant ionospheric feature is known as the equatorial or Appleton anomaly (Appleton, 1946).

The low-latitude ionosphere at F-region heights has been studied quite extensively in the last three decades for its electrodynamics and resultant ionospheric features (Blanc and Richmond, 1980; Fejer, 1986, 1991). Mainly from the Jicamarca (11.95° S; 76.87° W, geographic) experimental data, the various important characteristics of the vertical F-region plasma drift are well known today (Fejer et al., 1991). From the model results of SUPIM, the behavior of equatorial plasma fountain and equatorial anomaly is well understood (Balan and Bailey, 1995; Balan et al., 1997 and Bailey et al., 1997).

1.2 Vertical $\boldsymbol{E} \times \boldsymbol{B}$ drift velocity variations

As the Jicamarca data indicate (Fejer, 1991), the magnitude of the vertical F-region $\boldsymbol{E} \times \boldsymbol{B}$ plasma drift velocity largely depends upon various geophysical factors, such as the levels of magnetic activity, the phase of the solar cycle and the seasons. The diurnal pattern of the vertical upward $\boldsymbol{E} \times \boldsymbol{B}$ drift velocity variations in time is such that a day-time velocity peak ($\sim$20 m/s) is reached at around 11:00 LT. Following this day-time peak, the vertical upward $\boldsymbol{E} \times \boldsymbol{B}$ drift velocity decreases to a day-time minimum of approximately 10 m/s attained at around 16:00 LT. Then, the vertical upward $\boldsymbol{E} \times \boldsymbol{B}$ drift velocity suddenly increases to an evening maximum of 40–50 m/s soon after sunset (at around 19:00 LT). This event is called the pre-reversal or evening enhancement. Following that the vertical upward $\boldsymbol{E} \times \boldsymbol{B}$ drift velocity rapidly decreases through 0 m/s (at around 19:50 LT), where it becomes downward directed, to a negative maximum of 30–40 m/s (at around 21:00 LT). Finally, the vertical downward $\boldsymbol{E} \times \boldsymbol{B}$ drift velocity increases back to 0 m/s and reverses its direction back to vertical upward from vertical downward at around local sunrise. This typical 24-h trend can be largely modified by the seasonal and solar cycle variations. While the day-time drift velocity values show less variation with the changing seasons and solar activities, the night-time downward velocities exhibit a large variability. The pre-reversal enhancement of the vertical upward $\boldsymbol{E} \times \boldsymbol{B}$ plasma drift velocity is most obvious during the equinoctial and summer seasons at low sunspot numbers, and during all the seasons at high sunspot numbers (Fejer et al., 1991).

1.3 Vertical $\boldsymbol{E} \times \boldsymbol{B}$ drift velocity events and resultant ionospheric features identified by SUPIM

The ionospheric processes, related to the evening variations of the vertical upward $\boldsymbol{E} \times \boldsymbol{B}$ drift velocity, are identified by the model results of SUPIM (Balan and Bailey, 1995; Balan et al., 1997; Bailey et al., 1997). The three main events of the evening variations of the vertical upward $\boldsymbol{E} \times \boldsymbol{B}$ drift velocity are the pre-reversal enhancement, the reversal and the downward maximum. The event of pre-reversal enhancement is related to the evening maximum of the vertical upward $\boldsymbol{E} \times \boldsymbol{B}$ drift velocity ($\uparrow \boldsymbol{E} \times \boldsymbol{B}$ = max). The event of reversal occurs when the vertical upward $\boldsymbol{E} \times \boldsymbol{B}$ drift velocity is zero ($\uparrow \boldsymbol{E} \times \boldsymbol{B} = 0$) and becomes downward directed ($\downarrow \boldsymbol{E} \times \boldsymbol{B} \geq 0$). At downward maximum, the vertical downward $\boldsymbol{E} \times \boldsymbol{B}$ drift velocity is maximum ($\downarrow \boldsymbol{E} \times \boldsymbol{B}$ = max). During these $\boldsymbol{E} \times \boldsymbol{B}$ drift velocity events, the ionospheric processes taking place are different. Thus, the equatorial plasma fountain operates differently. While the vertical $\boldsymbol{E} \times \boldsymbol{B}$ drift velocity is upward and positive ($\uparrow \boldsymbol{E} \times \boldsymbol{B} > 0$), the equatorial plasma fountain is a forward fountain. Soon after the reversal of the vertical upward $\boldsymbol{E} \times \boldsymbol{B}$ drift velocity ($\uparrow \boldsymbol{E} \times \boldsymbol{B} = 0$), the equatorial forward plasma fountain becomes a reverse plasma fountain. While the $\boldsymbol{E} \times \boldsymbol{B}$ drift velocity is downward directed ($\downarrow \boldsymbol{E} \times \boldsymbol{B}$), the equatorial plasma fountain operates in a reverse manner and becomes a reverse fountain (Balan and Bailey, 1995; Balan et al., 1997; Bailey et al., 1997).

The ionospheric formations resulting from the evening variations of the vertical upward $\boldsymbol{E} \times \boldsymbol{B}$ drift velocity were also investigated with the model results of SUPIM (Balan and Bailey, 1995; Balan et al., 1997; Bailey et al., 1997). These resultant ionospheric features identified by SUPIM: are the symmetrical equatorial anomaly with plasma bubbles when $\uparrow \boldsymbol{E} \times \boldsymbol{B}$ = max, the broken down equatorial anomaly with plasma bubbles when $\uparrow \boldsymbol{E} \times \boldsymbol{B} = 0$, and the symmetrical equatorial peak when $\downarrow \boldsymbol{E} \times \boldsymbol{B}$ = max. As is well known from the published model results of SUPIM, the equatorial anomaly is created by the forward plasma fountain. At the evening enhancement of the vertical upward $\boldsymbol{E} \times \boldsymbol{B}$ drift velocity, when the vertical upward $\boldsymbol{E} \times \boldsymbol{B}$ drift velocity quickly increases to an evening maximum ($\uparrow \boldsymbol{E} \times \boldsymbol{B}$ = max), the equatorial forward plasma fountain undergoes a pre-reversal strengthening. Thus, the resultant ionospheric feature of the forward plasma fountain is a well-developed and symmetrical equatorial anomaly with plasma bubbles appearing at the crest and trough regions. At the reversal, when the magnitude of vertical upward drift velocity rapidly drops down to zero ($\uparrow \boldsymbol{E} \times \boldsymbol{B} = 0$) and its direction becomes opposite ($\downarrow \boldsymbol{E} \times \boldsymbol{B} > 0$), this well-developed and symmetrical equatorial anomaly suddenly breaks down. During the breaking down process, the development of large plasma bubbles takes place at the crest and trough regions. This breaking down process of the equatorial anomaly continues while the reverse fountain operates. At the strongest stage of the process, when the vertical downward $\boldsymbol{E} \times \boldsymbol{B}$ drift velocity is maximum ($\downarrow \boldsymbol{E} \times \boldsymbol{B}$ = max), the broken down equatorial anomaly transforms into a symmetrical equatorial night-time peak (Balan and Bailey, 1995; Balan et al., 1997; Bailey et al., 1997).

1.4 Aim and method of investigation

The main objective of this paper is to document the events of vertical $\boldsymbol{E} \times \boldsymbol{B}$ drift velocity variations with the TOPEX and GPS TEC data, to observe the effects of various $\boldsymbol{E} \times \boldsymbol{B}$ events on the low- and mid-latitude ionosphere, and to study some of the physical processes underlying the $\boldsymbol{E} \times \boldsymbol{B}$ events investigated. Observation of the low-latitude ionospheric irregularities associated with these $\boldsymbol{E} \times \boldsymbol{B}$ events utilizing the GPS data, and investigation of the effects of those low-latitude

Table 1. List of (top one) GPS ground-based receiver, (middle two) ground magnetometer and (bottom one) ionosonde station sites used for data collection

Station	Geographic		Geomagnetic	
	Longitude (° E)	Latitude (° N)	Longitude (° E)	Latitude (° N)
Guam	144.86	13.59	215.55	5.63
Muntinlupa	121.02	14.37	191.57	3.58
Lunping	121.17	25.00	189.50	13.80
Port Moresby	147.10	−9.40	219.20	−18.30

ionospheric irregularities on the dual-frequency GPS signal recordings are also objectives.

In order to achieve these goals, the high sunspot number 1998–1999 TOPEX and GPS satellite data, and the low sunspot number 1995 TOPEX satellite data were reduced to TEC (total electron content) values in TEC units (1 TECU=10^{+16} e^-/m^2). The dual frequency GPS technique, which makes use of two closely spaced L-band (L_1 = 1575.42 MHz; L_2 = 1227.60 MHz) frequency radio signals transmitted from the GPS satellites in multiple directions, provided the differential time delay ($\delta\Delta$T in seconds) and differential carrier phase advance ($\delta\Delta\phi$ in cycles) GPS satellite data. By applying the TEC theory, the raw GPS satellite data were used to calculate at first the slant GPS TEC values that were subsequently converted into vertical GPS TEC values (Klobuchar, 1996). As the GPS satellites revolve around the Earth in circular 12-h orbits at an altitude of 20 183 km, the satellites come into the visible range of the ground-based receiver twice a day for approximately 7 h, which is the length of time of a complete GPS satellite pass. There are six orbital planes of the GPS satellites around the Earth, where each plane is spaced 60° apart and inclined at 55°. The dual frequency (13.65 GHz and 5.3 GHz) TOPEX technique provided the over-the-ocean vertical TOPEX TEC values directly from the differential time delay measurements ($\delta\Delta$T in seconds) of the onboard altimeter that operates at nadir direction. At an inclination of 66°, the low-altitude (1335 km) satellite of the TOPEX/Poseidon mission covers the Earth in an approximately a 10-day cycle. A TOPEX cycle is made up of a total of 254 descending (or southbound) and ascending (or northbound) passes, where the time length of any pass is 0.935 h or 56 min and 6 s (Johnson et al., 1996).

In this study, the TOPEX and GPS TEC data were plotted in many different ways, which permitted the observation of many large- and small-scale (width ≤15° in latitude) ionospheric features globally over the oceans and locally in the Australian longitude region. Since the larger part of the Earth is covered by oceans, the global TOPEX TEC maps constructed with the over-the-ocean TOPEX TEC values provide an excellent means to observe the large-scale ionospheric features worldwide. The individual TOPEX TEC passes, plotted in geographic and geomagnetic latitudes, made it possible to view both the large- and small-scale ionospheric features at low- and mid-latitudes. The GPS TEC data from Guam (215.55° E; 5.63° N, geomagnetic; see also Table 1), situated close to the magnetic equator in the Australian longitude region, were plotted in time and geographic latitudes to observe the small-scale ionspheric features at low-latitudes. TOPEX passes situated close to the Australian East Coast could be matched up with the Guam GPS TEC plots, as the Guam data cover the northern crest of the equatorial anomaly. The effects of low-latitude ionospheric irregularities on the GPS recordings were documented with the raw GPS TEC data and the intensity of signal degradation was shown with the filtered Guam GPS dTEC/min or 1-min GPS TEC data in TECU. By adopting the technique of Chandra and Rastogi (1974), the daily variations of vertical $\boldsymbol{E} \times \boldsymbol{B}$ drift velocity were observed with the ΔH (nT) parameter at 121° E geographic longitude. H is the horizontal intensity (H) of the geomagnetic field (B) measured in nano (n or 10^{-9}) Teslas (T). H reflects the changes in the equatorial plasma fountain when measured at the magnetic dip equator ($H_{equator}$). All the non-ionospheric variations can be eliminated from the $H_{equator}$ data, if the H variations away from the equator ($H_{non-equator}$) are removed. Thus, the net parameter obtained and called ΔH or $H_{equator}$-$H_{non-equator}$ is a good indicator of the vertical $\boldsymbol{E} \times \boldsymbol{B}$ drift velocity. For this paper, the equatorial Muntinlupa (191.57° E; 3.58° N, geomagnetic; see Table 1) and non-equatorial Lunping (189.50° E; 13.80° N, geomagnetic; see Table 1) magnetometer data were used to obtain the ΔH parameter. For studying the physical background of the various vertical $\boldsymbol{E} \times \boldsymbol{B}$ drift velocity events in the low-latitude F-region ionosphere at the Australian longitude region, the virtual height or h'F (Km) ionosonde data from Port Moresby (147.10° E; −9.40° N, geographic; see Table 1) were utilized. Port Moresby is situated close to the southern crest of the equatorial anomaly in the Australian longitude region.

2 Results and discussion: vertical $\boldsymbol{E} \times \boldsymbol{B}$ drift velocity events and plasma fountain behavior observed

2.1 Forward plasma fountain

The forward plasma fountain is generated by the vertical upward $\boldsymbol{E} \times \boldsymbol{B}$ drift velocity and is symmetric with respect to the magnetic dip equator in the absence of neutral winds (Balan and Bailey, 1995). The working mechanism of the forward plasma fountain is such that it starts developing at around 09:00 LT, when the F-region vertical upward $\boldsymbol{E} \times \boldsymbol{B}$ drift

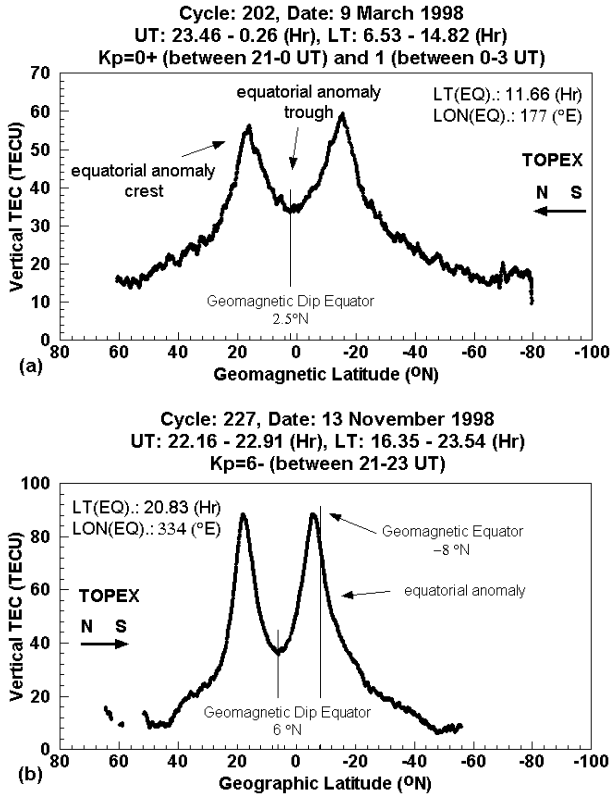

Fig. 1. The TOPEX TEC plots show the equatorial anomaly **(a)** in geomagnetic latitudes at 177° E (geographic), where the offset between the geomagnetic and dip equators is small and **(b)** in geographic latitudes at 334° E (geographic), where this offset is larger. (LT(EQ) = geographic equator crossing local time, LON(EQ) = equator crossing longitude, geographic, the arrow indicates the satellite travelling direction).

starts increasing. This vertical upward $\boldsymbol{E} \times \boldsymbol{B}$ drift, created by the combination of day-time eastward horizontal electric field (E) and the north-south horizontal magnetic field (B) at geomagnetic dip equator latitudes, drives the plasma across the horizontal magnetic field lines. In the equatorial region, the F2-region plasma rises until it loses momentum and then diffuses down the magnetic field lines and away from the magnetic dip equator due to the forces of gravity and pressure gradient. The overall process results in the formation of the equatorial ionization anomaly characterized by a trough centered over the geomagnetic dip equator, and two crests at about $\pm 17°$ magnetic latitudes in those longitude regions where the geomagnetic equator and geomagnetic dip equator overlap. An example of this is shown in Fig. 1a with a TOPEX pass where the TOPEX TEC is plotted against the geomagnetic latitudes. The negative geomagnetic latitude values indicate Southern Hemisphere latitudes. On 9 March 1998, the equatorial anomaly appeared over the western Pacific Ocean, close to the Australian East Coast, at 177° E geographic longitude at 11:66 LT, in decimal hours that is 11 h 39 min. Since the dip equator is situated at 2.5° north of the geomagnetic equator, the offset between the geomagnetic equator and geomagnetic dip equator is small, only 2.5° (latitude). If the offset between the geomagnetic and dip equators is large, one equatorial anomaly crest will be situated close to or on the geomagnetic equator, depending upon the magnitude of the offset, as the equatorial anomaly is symmetrical to the geomagnetic dip equator. In order to show this, a TOPEX pass over the eastern Atlantic Ocean at 334° E geographic longitude is plotted in geographic latitudes in Fig. 1b. The equatorial anomaly appeared on 13 November 1998 at 20:83 LT, in decimal hours that is 20 h 55 min. In this longitude region, the geomagnetic equator is 8° south of the geographic equator. As the geomagnetic dip equator is situated 6° north of the geographic equator, the offset is large, 14° (latitude). Thus, the southern crest of the equatorial anomaly is close to the geomagnetic equator.

The diurnal variations of the equatorial anomaly, on a global scale, is demonstrated with a series of global TOPEX TEC maps constructed with the low sunspot number 1995 Southern Hemisphere summer and autumnal equinox data for the day-time sector that extends from 09:50 LT to 17:50 LT at the geographic equator (denoted as LT(EQ) = equator crossing local time in hours (h), see Fig. 2). The TOPEX map with the earliest equator-crossing local time (09:50 LT; see Fig. 2a) shows that the asymmetrical equatorial anomaly appears first over the eastern Pacific Ocean, where the offset between the geomagnetic and geographic equators is increasing from the 200° E geographic longitude where they cross. As Balan et al. (1997) and Bailey et

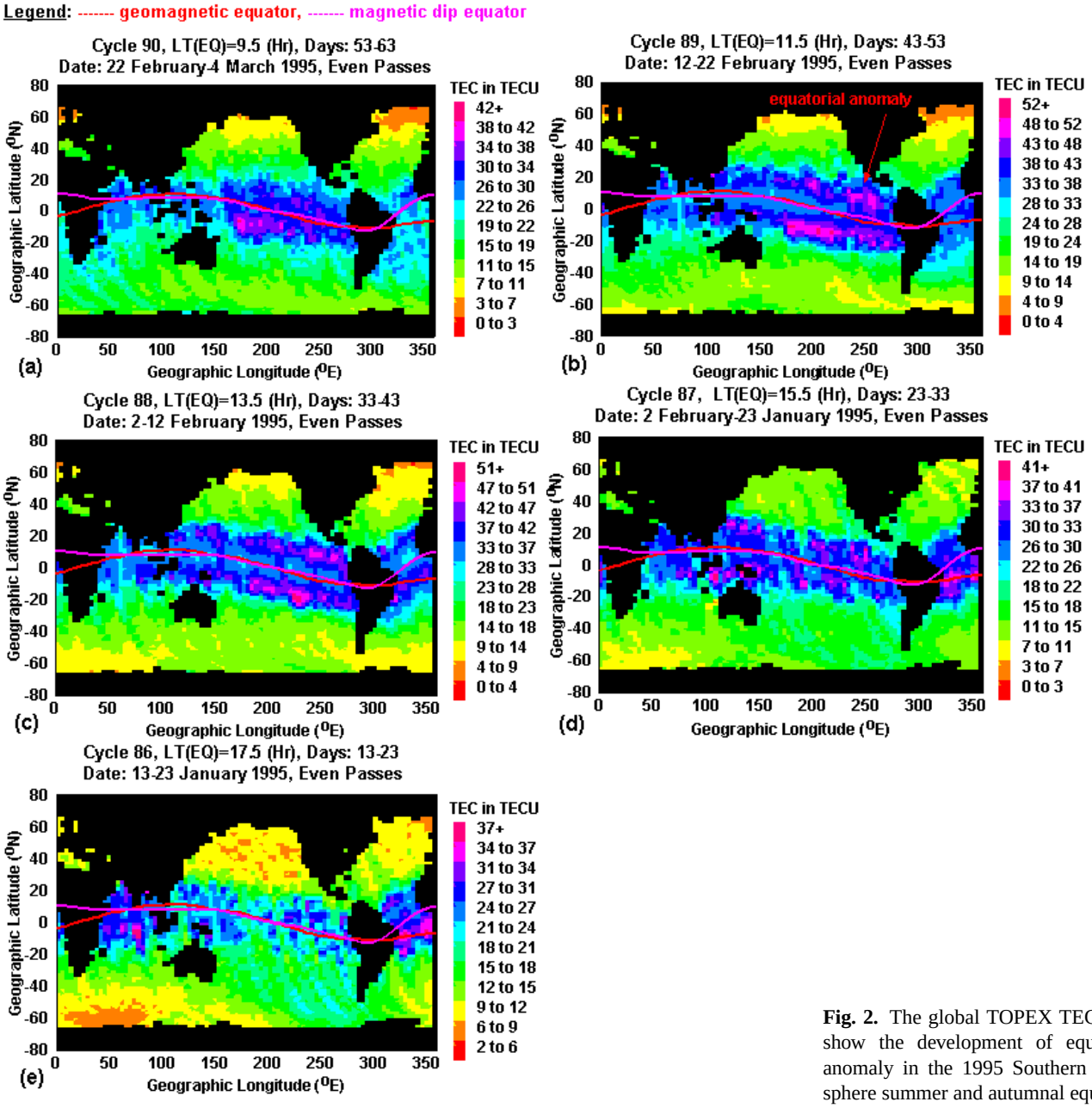

Fig. 2. The global TOPEX TEC maps show the development of equatorial anomaly in the 1995 Southern Hemisphere summer and autumnal equinox.

al. (1997) explained, the strong poleward wind makes the day-time equatorial anomaly highly asymmetrical in such a way that the plasma fountain extends to higher latitudes and supplies more ionization to the hemisphere with stronger poleward winds. Over the Pacific Ocean, the build up of the equatorial anomaly continues in the local morning and its best development occurs at around local midday (see Fig. 2b), when the upward $\boldsymbol{E} \times \boldsymbol{B}$ drift reaches its maximum day-time value. During the early and mid-afternoon hours (see Figs. 2c–d), the equatorial anomaly becomes better developed in the Australian longitude region and over the Atlantic Ocean. Later in the afternoon, the equatorial anomaly remains well developed over the Atlantic Ocean (see Fig. 2e). Furthermore, it becomes better developed over the Indian Ocean, and weaker over the Pacific Ocean and in the Australian longitude region (see Fig. 2e).

2.2 Pre-reversal strengthening of the vertical $\boldsymbol{E} \times \boldsymbol{B}$ drift velocity: $\uparrow \boldsymbol{E} \times \boldsymbol{B} = \max$

2.2.1 Model results with SUPIM

The vertical upward $\boldsymbol{E} \times \boldsymbol{B}$ drift velocity undergoes a pre-reversal enhancement soon after sunset. This can be explained by the eastward neutral winds, which blow across the east-west conductivity gradient and cause an enhancement of the eastward electric field (E) at around sunset. At this time, the effect of neutral wind upon the plasma foun-

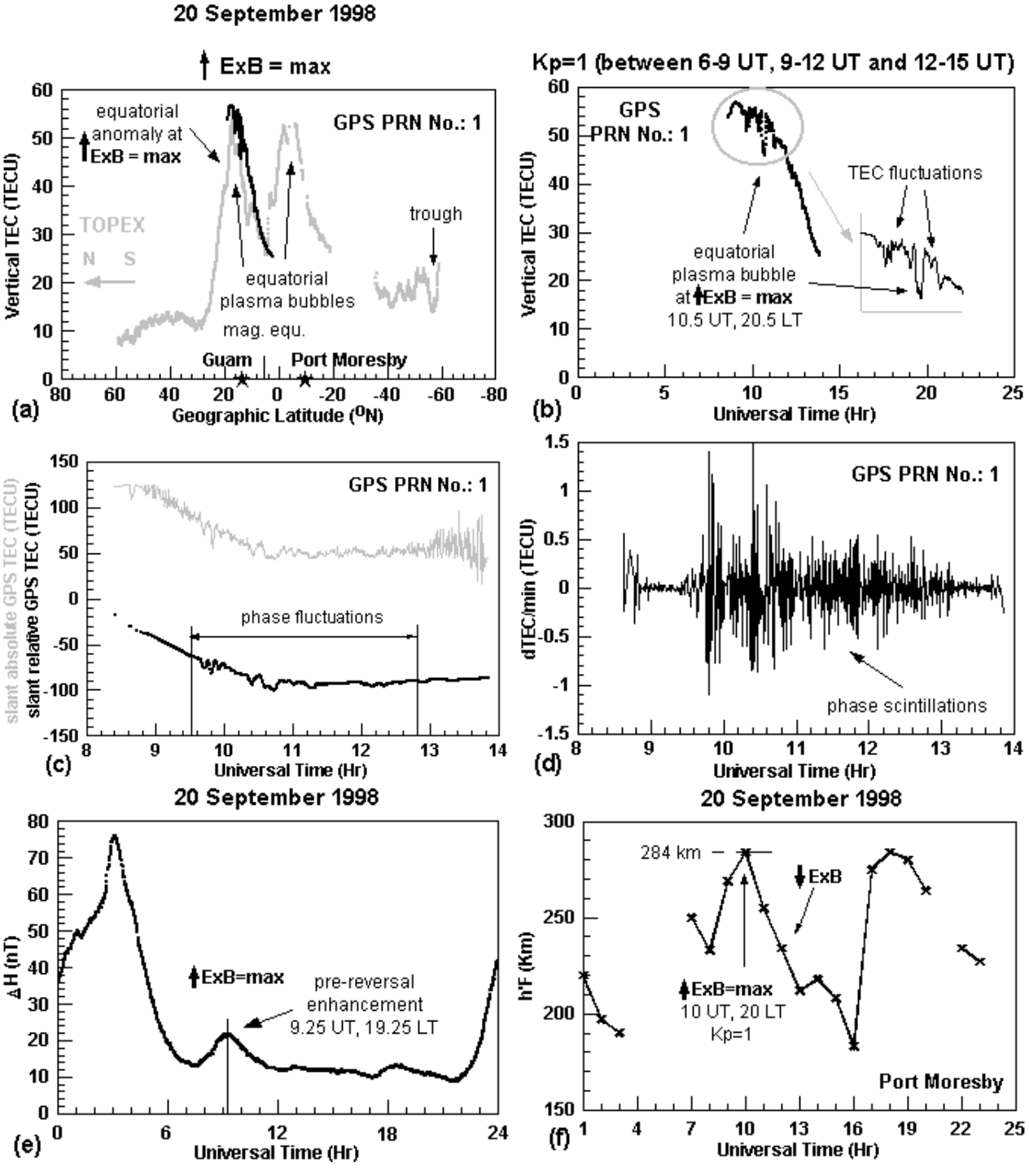

Fig. 3. The Guam GPS data show equatorial plasma bubbles **(a)** with the matching TOPEX TEC curve in latitudes (at 157° E, LT=20.20 h at the magnetic equator in decimal hours) and **(b)** in time. **(c)** Signal degradation on the raw GPS TEC data is due to the GPS phase scintillation. **(d)** The filtered dTEC/min plot shows the intensity of that phase scintillation. **(e)** The ΔH data plot obtained with the Muntinlupa and Lumping magnetic data shows the time of pre-reversal strengthening at 121° E geographic longitude, in the Australian region. **(f)** The data from Port Moresby show the sudden increase in height due to the pre-reversal strengthening, and then the sudden decrease due to the reversal and downward drift. The GPS satellite is distinguished by the PRN (Pseudo Random Noise) number. In the Australian region LT=UT+10 h.

tain is minimal due to the impulsive response of the ionosphere to the sudden strengthening of the F-region drift. This means that regardless of the longitudinal location, the forward plasma fountain becomes symmetric with respect to the geomagnetic dip equator. With the model results of SUPIM, Balan and Bailey (1995) and Balan et al. (1997) investigated the forward plasma fountain undergoing a pre-reversal strengthening at three different locations. Their results show that the above-mentioned impulsive response of the ionosphere drives the plasma to higher altitudes, which causes the plasma density to become largely reduced in the bottomside F-region. This leads to the development of plasma bubbles and spread-F irregularities via the Rayleigh-Taylor gradient instability in the region of the magnetic dip equator (Fejer and Kelley, 1980; Balan and Bailey, 1995; Balan et al., 1997).

2.2.2 Experimental observations

During the 1998 Southern Hemisphere vernal equinox season, the above mentioned events and their signatures were observed with the GPS and TOPEX TEC, magnetic and ionosonde data. Two examples are shown on the quiet days of 20 September 1998 (see Fig. 3) and 23 September 1998 (see Fig. 4). The resultant ionospheric features of the pre-reversal enhancement of the vertical upward $\boldsymbol{E} \times \boldsymbol{B}$ drift velocity was observed with the overlapping Guam GPS TEC and TOPEX TEC data plotted in geographic latitude (see Fig. 3a). On 20 September 1998, Fig. 3a shows the symmetrical equatorial anomaly with plasma bubbles at both crests with the TOPEX TEC data. The matching Guam GPS TEC plot shows also the plasma bubbles at the northern crest of this equatorial anomaly (see Fig. 3a). As the symbol $\star$ at 13.59° N geographic latitude indicates, in the Australian longitude region Guam is situated at the northern anomaly crest. The time of the bubble appearance was obtained with the same Guam GPS TEC data plotted in universal time (UT in hours; see Fig. 3b). In Eastern Australia the local time (LT in hours) is UT+10 hours. The GPS signal degradation, due to the development of equatorial plasma bubbles and small-scale ionospheric irregularities such as TEC fluctuations, is obvious on the raw Guam GPS TEC data, which are represented with the slant absolute and relative Guam GPS TEC curves (see Fig. 3c). The magnitude of this GPS signal degradation is illustrated with the filtered Guam GPS dTEC/min data (see Fig. 3d). It is worth noting that the GPS phase scintillation is quite strong during this magnetically quiet period ($K_p = 1$) at high sunspot numbers, when the Sun is more active. The GPS phase scintillations are a major concern today since they affect and degrade the performance of satellite links. The time of pre-reversal enhancement of the vertical upward $\boldsymbol{E} \times \boldsymbol{B}$ drift velocity was estimated with the ΔH parameter plotted in time (see Fig. 3e) and it happened at around 09:25 UT or 19:25 LT in decimal hours. This pre-reversal enhancement sets the plasma into motion and therefore suddenly increases the F-region height. The event of F-region height increase is documented with the h'F data (see Fig. 3f) from Port Moresby, situated at the southern crest of the equatorial anomaly (indicated by the symbol $\star$ at $-9.40°$ N geographic latitude on Fig. 3a) in the Australian longitude region. This h'F plot shows the sudden increase in height at the time of pre-reversal enhancement of the vertical upward $\boldsymbol{E} \times \boldsymbol{B}$ drift velocity. As the Rayleigh-Taylor mode becomes unstable, due to the sudden height increase, the equatorial plasma bubbles develop (Fejer and Kelley, 1980) and cause the phase scintillations of the GPS signals. Since the plasma fountain is instantaneous, there is little time difference between the time of height rise and the time of the pre-reversal enhancement of the vertical upward $\boldsymbol{E} \times \boldsymbol{B}$ drift velocity. However, the resultant ionospheric features, such as the symmetrical equatorial anomaly and the plasma bubbles, have a time cumulative nature, and, therefore, they appear later in time.

2.2.3 Ionosphere-plasmasphere coupling governed by the eastward electric field

Figure 4 shows the same $\uparrow \boldsymbol{E} \times \boldsymbol{B}$ = max event with the 23 September 1998 data sets. However, the significance of this figure is that the TOPEX pass shown in Fig. 4a is field-aligned. It means that the ground track of this TOPEX satellite pass, obtained by plotting the geographic coordinates of the data points making up that TOPEX pass, follows the same magnetic field line. This field-aligned TOPEX pass shows that when the equatorial anomaly undergoes a pre-reversal strengthening, the TEC at mid-latitudes becomes depleted and, therefore, appears to be low in both hemispheres (indicated as "low TEC" in Fig. 4a). The development of low TEC at mid-latitudes is due to the ionosphere-plasmasphere coupling governed by the eastward electric field that was first explained by Park (1971).

The coupling of ionosphere and plasmasphere is governed by the electric fields in the ionosphere (E), which cause the vertical plasma movement via the vertical $\boldsymbol{E} \times \boldsymbol{B}$ drift that was introduced and explained in detail earlier in this paper. Park (1971) explained the background mechanisms with the height rise, caused by the increased eastward electric field lifting the ionosphere to higher altitudes where the loss rates are smaller, and with the reduced downward plasma flow from the plasmasphere to the ionosphere at mid-latitudes. These mechanisms create an initial decrease in the electron concentration, and, therefore, in the TEC, at mid-latitudes. In Fig. 4a the field-aligned TOPEX pass shows the low- and mid-latitude ionosphere at the pre-reversal enhancement of the eastward electric field ($\uparrow \boldsymbol{E} \times \boldsymbol{B}$ = max), and provides direct evidence of the ionosphere-plasmasphere coupling by showing their characteristic signatures. These signatures are the well-developed and symmetric equatorial anomaly with plasma bubbles at low latitudes, and the low-TEC region at mid-latitudes in both hemispheres. The rest of Fig. 4 is similar to that of Fig. 3 that was explained in detail in the previous section. In brief, Fig. 4b shows the plasma bubble, developed on the northern crest of the equatorial anomaly, in time with the Guam GPS TEC data. The associated signal degrada-

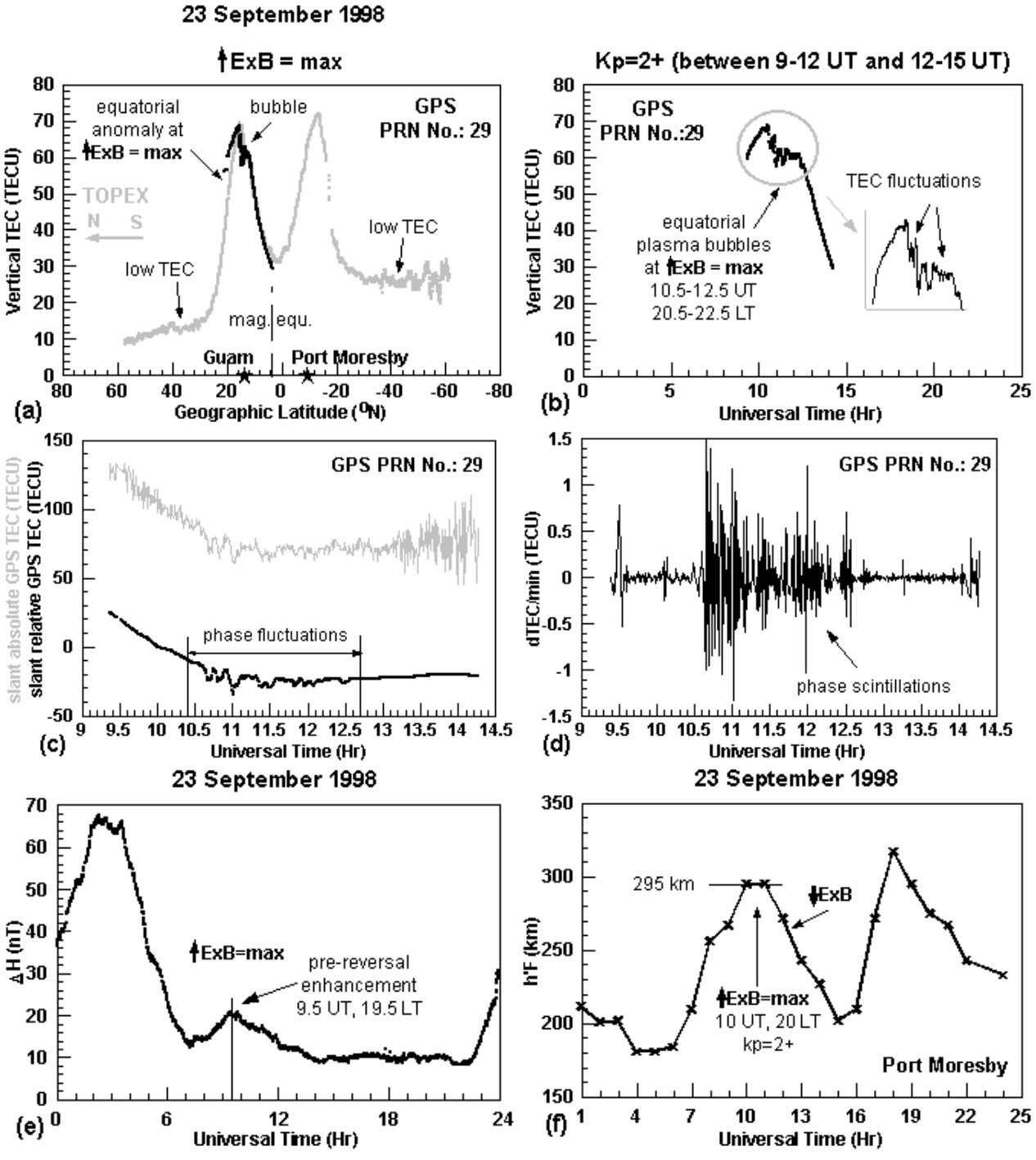

Fig. 4. The Guam GPS data show equatorial plasma bubbles **(a)** with the matching field-aligned TOPEX TEC curve (at 180° E, LT = 19:50 at the magnetic equator), which shows a mid-latitude low TEC region as well, in latitudes and **(b)** in time. **(c)** Signal degradation on the raw GPS TEC data is due to the GPS phase scintillation. **(d)** The filtered dTEC/min plot shows the intensity of that phase scintillation. **(e)** The ΔH data plot obtained with the Muntinlupa and Lumping magnetic data shows the time of pre-reversal strengthening at 121° E geographic longitude, in the Australian region. **(f)** The data from Port Moresby show the sudden increase in height due to the pre-reversal strengthening, and then the sudden decrease due to the reversal and downward drift.

tion on both GPS carriers are shown with Fig. 4c. Its magnitude is measured with the filtered Guam GPS dTEC/min data. As Fig. 4d shows, the intensity of GPS phase scintillation is obvious and quite intensive at high sunspot numbers for a magnetically quiet period ($K_p = 2+$). Finally, the time of evening enhancement was estimated with the ΔH parameter plotted in time in Fig. 4e, and the effect of the vertical upward plasma drift on the low-latitude ionosphere is shown with the sudden rise of h'F in Fig. 4f.

2.3 Vertical upward $\boldsymbol{E} \times \boldsymbol{B}$ drift velocity reversal: $\uparrow \boldsymbol{E} \times \boldsymbol{B} = 0$

2.3.1 Model results by SUPIM

Following the pre-reversal enhancement ($\uparrow \boldsymbol{E} \times \boldsymbol{B}$ = max), the vertical upward $\boldsymbol{E} \times \boldsymbol{B}$ drift velocity quickly decreases. In approximately 30 min, it reaches zero ($\uparrow \boldsymbol{E} \times \boldsymbol{B} = 0$), and then becomes negative ($\uparrow \boldsymbol{E} \times \boldsymbol{B} < 0$) or downward directed ($\downarrow \boldsymbol{E} \times \boldsymbol{B} > 0$). This event is called the $\boldsymbol{E} \times \boldsymbol{B}$ drift velocity reversal. At this time, the forward plasma fountain still diffuses downward along the magnetic field lines for a very short period of time. Soon after that, when the vertical upward $\boldsymbol{E} \times \boldsymbol{B}$ drift velocity becomes downward directed ($\downarrow \boldsymbol{E} \times \boldsymbol{B} > 0$), the reverse plasma fountain begins its operation (Balan and Bailey, 1995; Balan et al., 1997; Bailey et al., 1977). The $\boldsymbol{E} \times \boldsymbol{B}$ drift velocity reversal is caused by the ionospheric electric fields, which reverse to the west (from the east), as the day-time eastward neutral winds become westward directed after sunset. During the reversal, the large downward diffusion of the reverse plasma fountain provides favorable conditions for the generation and propagation of plasma bubbles and spread-F irregularities via the Rayleigh-Taylor gradient instability in the region of the magnetic dip equator (Fejer and Kelley, 1980). The neutral winds are most effective on the plasma fountain when the $\boldsymbol{E} \times \boldsymbol{B}$ drift velocity is zero (Balan and Bailey, 1995; Balan et al., 1997; Bailey et al., 1977). The resultant ionospheric features of the vertical upward $\boldsymbol{E} \times \boldsymbol{B}$ drift velocity reversal are the broken down equatorial anomaly, and the plasma bubbles at low-magnetic-equator-latitudes or at the equatorial anomaly trough and crests regions (Balan and Bailey, 1995; Balan et al., 1997; Bailey et al., 1977).

2.3.2 Experimental observations

All the above described events and their signatures were observed on the magnetically disturbed ($K_p = 6-$ and $5-$) day of 26 September 1998 with the Guam GPS and TOPEX TEC, magnetic and ionosonde data, which are shown in Fig. 5. In Fig. 5a the Guam GPS TEC values of a satellite pass, namely PRN (Pseudo Random Noise) number 1, are plotted in time and show two sets of equatorial plasma bubbles. These bubbles are related to the two different events of $\boldsymbol{E} \times \boldsymbol{B}$, which are associated with the development of plasma bubbles and small-scale ionospheric irregularities. The earlier set of bubbles belongs to the event of pre-reversal enhancement of the vertical upward $\boldsymbol{E} \times \boldsymbol{B}$ drift velocity ($\uparrow \boldsymbol{E} \times \boldsymbol{B}$ = max) and is situated at the northern crest of the equatorial anomaly. The latter set of bubbles is associated with the reversal of the drift velocity ($\uparrow \boldsymbol{E} \times \boldsymbol{B} = 0$) and is situated in the trough region of the equatorial anomaly. With the raw Guam GPS TEC data, the GPS signal degradation, due to the development of plasma bubbles and small-scale ionospheric irregularities, such as TEC fluctuations, is shown in Fig. 5b. Again, the magnitude of this GPS signal degradation is illustrated with the filtered Guam GPS dTEC/min (see Fig. 5c). During this magnetically disturbed period ($K_p = 6-$ and $5-$), the high intensity of the GPS phase scintillation is obvious. This Guam GPS dTEC/min plot also shows very clearly the two separate GPS phase scintillation events. As was explained before, the first event is related to the vertical upward $\boldsymbol{E} \times \boldsymbol{B}$ drift velocity increase before sunset, which is the pre-reversal enhancement (indicated as $\uparrow \boldsymbol{E} \times \boldsymbol{B}$ = max on Fig. 5c). The second event is the reversal (indicated as $\uparrow \boldsymbol{E} \times \boldsymbol{B} \approx 0$ on Fig. 5c). Figure 5c also clearly indicates that there is no phase scintillation between these two $\boldsymbol{E} \times \boldsymbol{B}$ events when the vertical upward $\boldsymbol{E} \times \boldsymbol{B}$ drift velocity quickly drops down to zero from positive maximum. The SUPIM model estimated 30-min time interval separating these two $\boldsymbol{E} \times \boldsymbol{B}$ events is longer on the filtered Guam GPS dTEC/min plot due to the time cumulative nature of the resultant ionospheric features, which are the plasma bubbles and TEC fluctuations at each event. In order to show the resultant ionospheric features at low- and mid-latitudes at each $\boldsymbol{E} \times \boldsymbol{B}$ event, the Guam GPS TEC pass in Fig. 5a was matched with two field-aligned TOPEX TEC cross sections. Figure 5d shows the ground tracks of the TOPEX satellite passes that were used in the construction of field-aligned TOPEX TEC cross sections. For the event pre-reversal enhancement ($\uparrow \boldsymbol{E} \times \boldsymbol{B}$ = max), the field-aligned TOPEX TEC cross section constructed with two TOPEX passes (see Figs. 5d and e) shows the symmetrical equatorial anomaly with plasma bubbles at both crests and the low TEC region at southern mid-latitudes. The bubble at the northern anomaly crest was also detected with the first set of bubbles in the Guam GPS TEC data, and the good match of the two different satellite data is apparent. At southern mid-latitudes, the TEC depletion, explained with the ionosphere-plasmasphere coupling (see detailed explanation in Sect. 2.2.3 Ionosphere-plasmasphere coupling governed by the eastward electric field), is obvious and indicated as "low TEC" in Fig. 5e. For the event of drift velocity reversal ($\uparrow \boldsymbol{E} \times \boldsymbol{B} = 0$), another field-aligned TOPEX TEC cross section was constructed with three TOPEX satellite passes (see Figs. 5d and f). Figure 5f shows the breaking down of the equatorial anomaly when the anomaly crests are broken down already, and the plasma bubbles in the anomaly trough region are still well developed. The second set of plasma bubbles in the Guam GPS data matches well with this field-aligned TOPEX TEC cross section and gives supportive evidence for the Guam GPS TEC data interpretation. This field-aligned TOPEX TEC cross section also reveals the appearance of mid-latitude night-time TEC increases in both hemispheres. Figure 5g shows the ΔH parameter plotted in

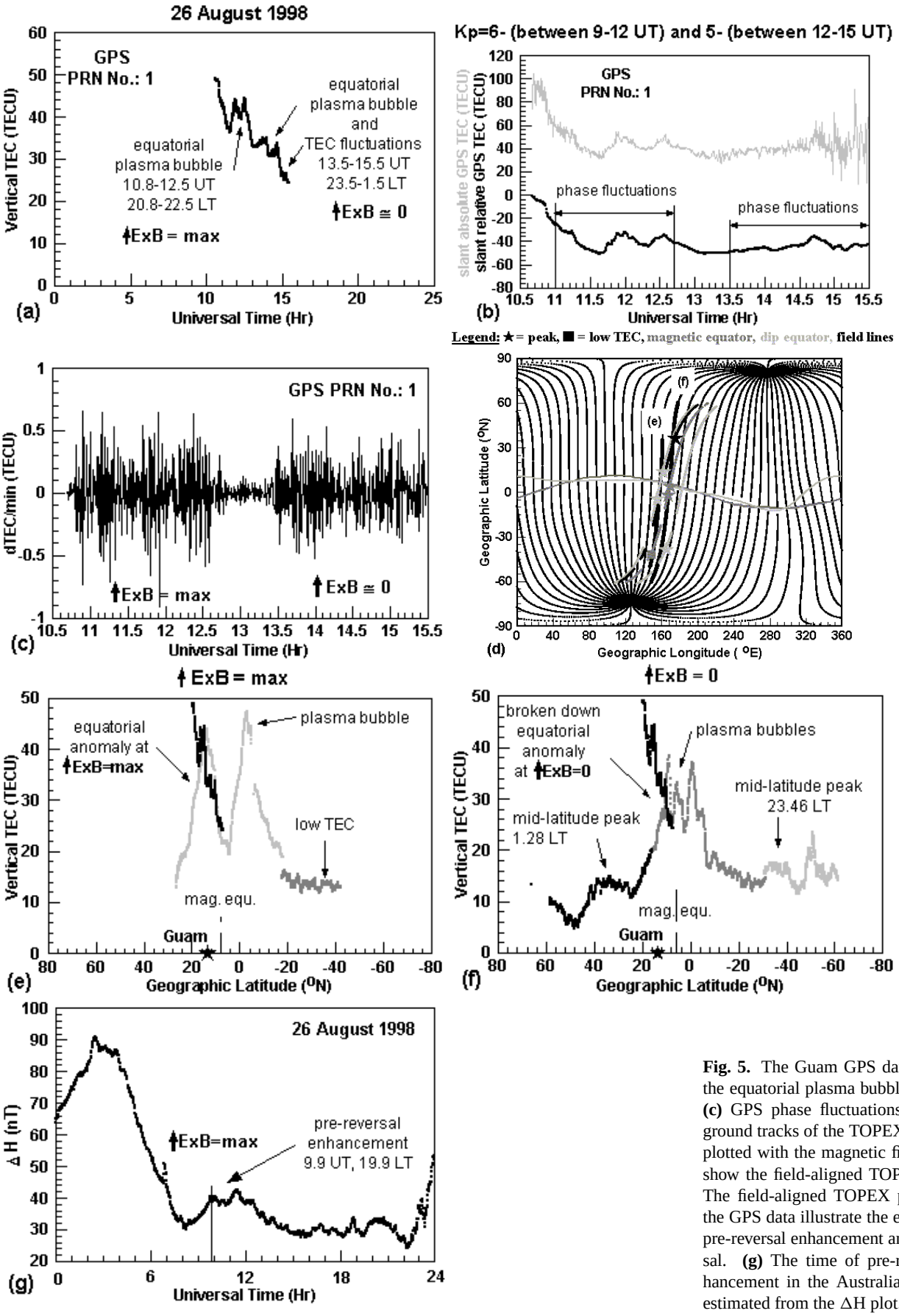

Fig. 5. The Guam GPS data show **(a)** the equatorial plasma bubbles and **(b)–(c)** GPS phase fluctuations. **(d)** The ground tracks of the TOPEX passes are plotted with the magnetic field lines to show the field-aligned TOPEX passes. The field-aligned TOPEX passes with the GPS data illustrate the events of **(e)** pre-reversal enhancement and **(f)** reversal. **(g)** The time of pre-reversal enhancement in the Australian region is estimated from the ΔH plot.

time for the day of 26 August 1998, to estimate the time of pre-reversal enhancement of the vertical upward $\boldsymbol{E} \times \boldsymbol{B}$ drift velocity. This happened at around 10:00 UT or 20:00 LT. The first set of Guam GPS phase scintillations, the signature of pre-reversal enhancement of the vertical upward $\boldsymbol{E} \times \boldsymbol{B}$ drift velocity, started at 0.75 h or 45 min later, at around 10:75 UT or 20:75 LT. This later occurrence is due to the time cumulative nature of the resultant ionospheric features.

2.3.3 Ionosphere-plasmasphere coupling governed by the westward electric field

The development of mid-latitude night-time TEC increases shown in Fig. 5f can be explained with the ionosphere-plasmasphere coupling governed by the westward electric field. According to Park (1971), at the time of vertical upward $\boldsymbol{E} \times \boldsymbol{B}$ drift velocity reversal ($\uparrow \boldsymbol{E} \times \boldsymbol{B} = 0$), a downward plasma flow from the plasmashere to the ionosphere at mid-latitudes in both hemispheres is triggered by the westward electric field. This mechanism results in the development of ionospheric night-time TEC increases at mid-latitudes in both hemispheres (see detailed explanation in Sect. 2.6 Development of mid-latitude night-time TEC increases).

2.4 Vertical downward $\boldsymbol{E} \times \boldsymbol{B}$ drift velocity between reversal and maximum: $0 < \downarrow \boldsymbol{E} \times \boldsymbol{B} < \max$

2.4.1 Model results by SUPIM

Soon after the reversal, the vertical upward $\boldsymbol{E} \times \boldsymbol{B}$ drift becomes downward directed, and the forward plasma fountain begins its operation in the opposite direction. The downward drift pushes the plasma down, across the horizontal magnetic field lines, which creates a low plasma pressure region in the topside ionosphere. As a response to the generation of this low-plasma-pressure region, the plasma starts flowing towards the magnetic equator, from both of the high-pressure crests, to fill up this low-pressure region. As the downward drift continues, it creates a new, low-pressure region at the magnetic equator and the process goes on until the intensity of the downward drift decreases. This mechanism is called the reverse fountain and it is responsible for the breaking down of the equatorial anomaly. The associated ionospheric feature at magnetic-equator-latitudes is an asymmetrical broken down equatorial anomaly. During this time, the neutral winds can alter the symmetry of the reverse plasma with respect to the magnetic equator (Balan and Bailey, 1995; Balan et al., 1997; Bailey et al., 1977).

2.4.2 Experimental observations

The event after the reversal and its signatures were observed with the TOPEX data on the magnetically quiet day of 27 October 1998. In Figs. 6a–c, two field-aligned TOPEX TEC cross sections situated over the Pacific Ocean are illustrated. Figure 6a shows the ground tracks of the satellite passes utilized and the magnetic field lines in the grid of geographic parallels. Figures 6b and c show the resultant ionospheric features of the reverse plasma fountain at such a stage when the vertical downward $\boldsymbol{E} \times \boldsymbol{B}$ drift velocity is between reversal and downward maximum ($0 < \downarrow \boldsymbol{E} \times \boldsymbol{B} < \max$). Both field-aligned TOPEX TEC cross sections show the asymmetrical broken down equatorial anomaly when the equatorial plasma bubbles developed at the reversal are gone already, and when the residue of the equatorial anomaly crests has almost disappeared. In both hemispheres, the mid-latitude night-time TEC increases at around $\pm 40^\circ$ N geomagnetic latitudes appear to be well developed. These field-aligned TOPEX passes indicate that the mid-latitude night-time TEC increases in both hemispheres are maintained during the operation of the reverse plasma fountain.

2.5 Maximum vertical downward $\boldsymbol{E} \times \boldsymbol{B}$ drift velocity: $\downarrow \boldsymbol{E} \times \boldsymbol{B} = \max$

2.5.1 Model results by SUPIM

The reverse plasma fountain becomes most intensive when the downward vertical $\boldsymbol{E} \times \boldsymbol{B}$ velocity drift reaches its maximum ($\downarrow \boldsymbol{E} \times \boldsymbol{B} = \max$) at around 21:00 LT. At that stage, the associated ionospheric feature at magnetic-equator latitudes is a night-time TEC increase centered over and symmetrical to the overlapping magnetic and dip equators. The main source of plasma building up the night-time increases at the magnetic-equator latitudes is the reverse fountain (Balan and Bailey, 1995; Balan et al., 1997; Bailey et al., 1997). During the time of maximum vertical downward drift, the neutral winds have the least effect on the reverse plasma fountain and, therefore, its symmetry is not altered (Balan et al., 1997).

2.5.2 Experimental observations

This $\downarrow \boldsymbol{E} \times \boldsymbol{B} = \max$ event and its signatures were observed on the very quiet day ($K_p = 0+$ and $1-$) of 19 March 1998 with a field-aligned TOPEX TEC pass shown in Fig. 7. Figure 7a illustrates the ground tracks of TOPEX passes used for constructing the field-aligned TOPEX pass. The resultant ionospheric feature of the reverse plasma fountain, when the vertical downward $\boldsymbol{E} \times \boldsymbol{B}$ drift velocity is maximum ($\downarrow \boldsymbol{E} \times \boldsymbol{B} = \max$), is shown in Fig. 7b. It is a symmetric night-time TEC increase centered over the overlapping magnetic and dip equators. This field-aligned TOPEX pass also shows a well-developed mid-latitude night-time TEC increase in the Southern Hemisphere at 41.89° N geographic or 36.75° N geomagnetic latitude and the conjugate TEC increase in the Northern Hemisphere. As the operation of reverse plasma fountain continues after the reversal and as the magnitude of vertical downward $\boldsymbol{E} \times \boldsymbol{B}$ drift velocity nears towards its maximum, the equatorial anomaly becomes more and more reduced. Finally, it turns into one single peak that is symmetrical, because the neutral winds have no effect on the reverse plasma fountain at maximum vertical downward drift. While the ionospheric electric field is westward directed, the mid-latitude night-time TEC increases in both hemispheres are

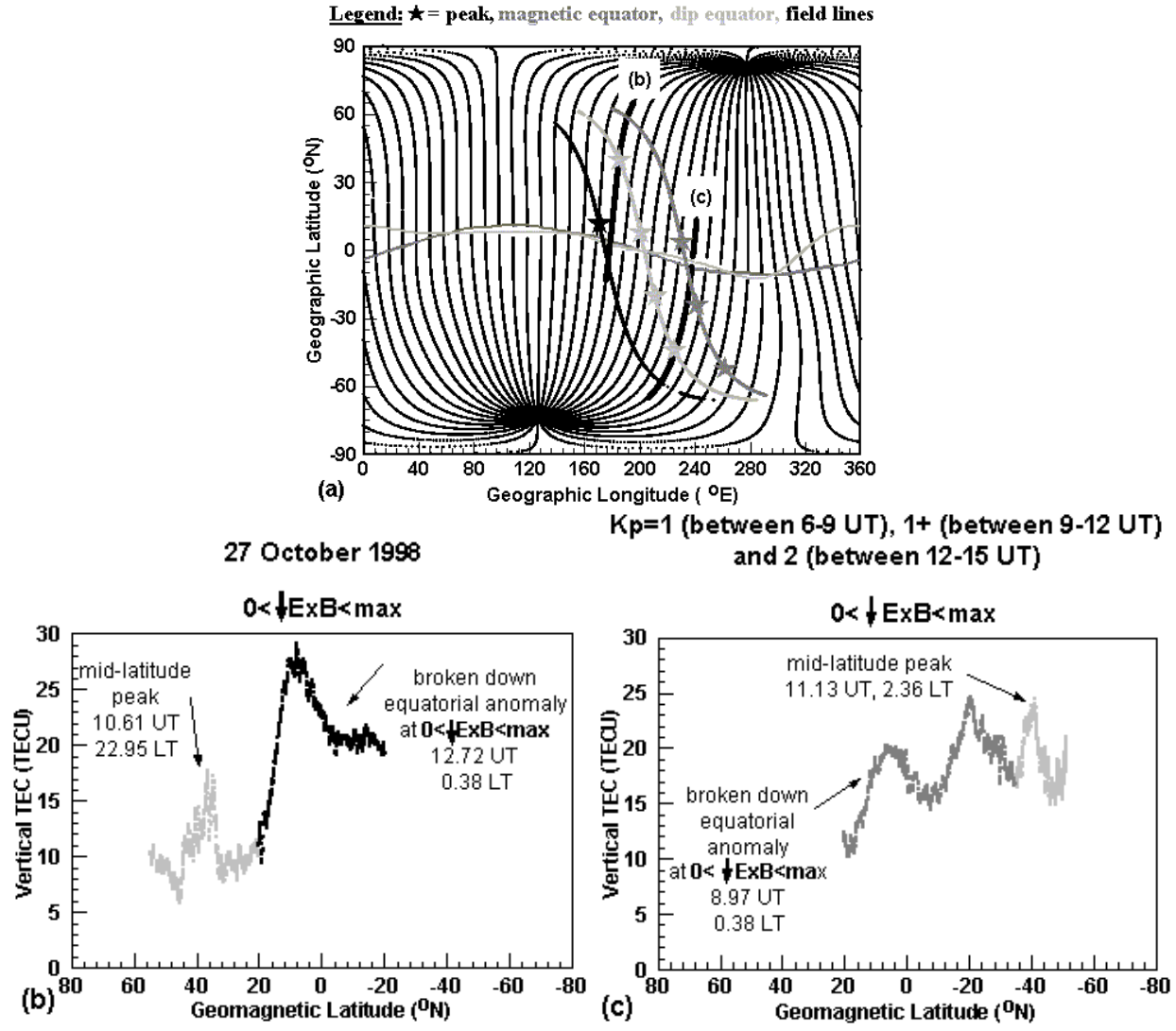

Fig. 6. (a) The ground tracks of the TOPEX passes are plotted with the magnetic field lines to show the field-aligned TOPEX passes. **(b)–(c)** The field-aligned TOPEX TEC cross sections depict the broken down equatorial anomaly at less than maximum downward drift and the mid-latitude night-time TEC increases.

maintained by the plasma flows from the plasmasphere to the ionosphere at mid-latitudes via the ionosphere-plasmasphere coupling governed at this time by the westward electric field.

2.6 Development of mid-latitude night-time TEC increases

With the various field-aligned TOPEX TEC cross sections presented in this paper, the absence and presence of night-time TEC increases at mid-latitudes were demonstrated at the various stages of the operation of forward and reverse plasma fountain. Based upon the work of Park (1971), the depletion of mid-latitude electron density, and hence the TEC, was explained with the eastward electric field via the ionosphere-plasmasphere coupling. The enhanced eastward electric field has the potential to reduce the mid-latitude downward plasma diffusion from the plasmasphere to the ionosphere at mid-latitudes in both hemispheres, and therefore to decrease the TEC at mid-latitudes (see Figs. 4a and 5e). This enhanced eastward electric field is also responsible for the stronger vertical upward $\boldsymbol{E} \times \boldsymbol{B}$ drift at magnetic-equator-latitudes that is known as the pre-reversal enhancement when the vertical upward $\boldsymbol{E} \times \boldsymbol{B}$ drift velocity is maximum ($\uparrow \boldsymbol{E} \times \boldsymbol{B}$ = max). The increased F-region heights at low-latitudes (see Fig. 4f) and decreased electron density, and therefore TEC, at mid-latitudes (see Figs. 4a and 5e) were interpreted to be the signatures of the $\uparrow \boldsymbol{E} \times \boldsymbol{B}$ = max event. Soon after sunset, when the eastward day-time neutral winds become westward directed, the eastward electric field turns westward. This westward electric field reverses the vertical $\boldsymbol{E} \times \boldsymbol{B}$ plasma drift from upward to downward, and at the reversal the drift velocity is zero ($\uparrow \boldsymbol{E} \times \boldsymbol{B} = 0$). Due to the coupling of the ionosphere and plasmasphere, the westward electric field triggers a plasma flow, from the plasmasphere to the ionosphere at mid-latitudes in both hemispheres, which is the

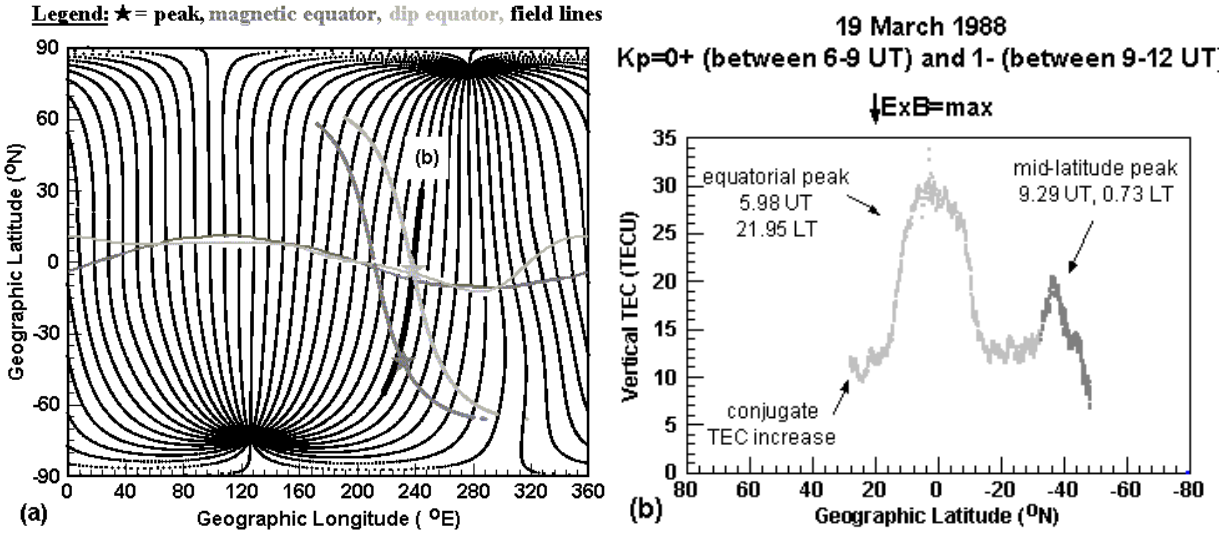

Fig. 7. (a) The ground tracks of the TOPEX passes are plotted with the magnetic field lines to show the field-aligned TOPEX pass. **(b)** The field-aligned TOPEX TEC cross section depicts the symmetric equatorial peak at maximum downward drift and the mid-latitude night-time TEC increases in magnetic latitudes.

main source of plasma building up the night-time TEC increases at mid-latitudes in both hemispheres. This plasma flow continues while the ionospheric electric field is westward directed and maintains the mid-latitude night-time TEC increases in both hemispheres during the vertical downward $\boldsymbol{E} \times \boldsymbol{B}$ drift ($0 > \downarrow \boldsymbol{E} \times \boldsymbol{B} \geq$max; see Figs. 6b–c and 7b) at magnetic-equator latitudes. The dramatic decrease of F-region heights at low-latitudes soon after the pre-reversal enhancement (see Figs. 3f and 4f), and the appearance (see Fig. 5f) and maintenance (see Figs. 6b–c and 7b) of conjugate night-time TEC increases at mid-latitudes are the signatures of the vertical downward $\boldsymbol{E} \times \boldsymbol{B}$ drift event.

As Park (1971) explained, the lowering of the night-time F-layer results in increased electron densities at mid-latitudes, which is a direct consequence of the westward electric field. The increased electron densities at mid-latitudes can be explained with the decreased height of the F-layer that creates an enhanced loss rate, which competes with the enhanced downward plasma flow from the plasmasphere to the ionosphere at mid-latitudes, triggered and maintained by the westward electric field. At greater heights, where the loss rates are smaller, the downward flowing plasma becomes a dominant factor and the lowering of the F-layer results in increased electron densities.

To explain this process in greater detail, the mechanism is as follows. By assuming that the ionization consists of O^+, H^+ and electrons in equilibrium, the vertical downward $\boldsymbol{E} \times \boldsymbol{B}$ drift velocity forces the ionosphere down to lower heights and therefore reduces the concentration of O^+ (i.e. $[O^+]$). Consequently, at a certain altitude, the $[O^+]$ has been reduced while [O] and [H] remained unaffected. The following reduction in $[H^+]$ (protons) creates a non-equilibrium gradient and also a downward diffusion of $[H^+]$. In this downward proton diffusion from the plasmasphere to the ionosphere at mid-latitudes, the $[O^+]$ increases by the charge exchange with the neutral oxygen: $H^+ + O \rightarrow H + O^+$. As a final result, the lowering of the F-layer at mid-latitudes is coupled with an increase in the electron concentration and TEC at mid-latitudes (Park, 1971).

3 Summary and conclusion

Based upon the published SUPIM results (Balan and Bailey, 1995; Balan et al., 1997; Bailey et al., 1997), the development of forward and reverse plasma fountain, their behavior, and the working mechanism of the forward and reverse plasma flows were discussed and illustrated with experimental data at various K_p values. Since the magnetic forces have a great importance in the development of the resultant ionospheric features at magnetic-equator-latitudes and mid-latitudes, the field-aligned TOPEX passes were used for the investigation. With these "field-aligned" TOPEX TEC cross sections, constructed by connecting two or three different TOPEX passes that cross the same magnetic field lines, the various $\boldsymbol{E} \times \boldsymbol{B}$ drift velocity events were documented and the behavior of the plasma fountain was followed up. The typical ionospheric signatures of each event at magnetic-equator-latitudes were noted and the good agreement between the model results of SUPIM and experimental TOPEX results was found. In the Australian longitude region, the associated low-latitude ionospheric irregularities, such as plasma bubbles and TEC fluctuations, were observed with the Guam GPS TEC data that cover the northern crest of the equatorial anomaly. Their effects on the dual-frequency GPS car-

riers were demonstrated with the raw Guam GPS TEC data. The magnitude of the associated strong GPS phase fluctuations was measured and demonstrated with the filtered Guam GPS dTEC/min plots. Even during the magnetically quiet periods investigated, the severe signal degradation at high sunspot numbers was obvious and was explained with the ionospheric irregularities formed at a more intensive solar activity. The effects of plasma fountain on the equatorial ionosphere were studied with the virtual height or h'F ionosonde data from Port Moresby situated at the southern crest of the equatorial anomaly in the Australian longitude region. The sudden F-region height rise at the time of pre-reversal enhancement and fall at the reversal were all obvious. The time of the pre-reversal enhancement of the vertical upward $\boldsymbol{E} \times \boldsymbol{B}$ drift velocity was estimated with the ΔH parameter. The similar time values obtained with the h'F and ΔH data indicate the instantaneous nature of the plasma fountain. However, the later occurrence of resultant ionospheric features can be explained with their time cumulative nature.

The field-aligned TOPEX TEC cross sections made it possible to observe the mid-latitude ionosphere at the time of each $\boldsymbol{E} \times \boldsymbol{B}$ drift velocity event. The various examples at low and high K_p values indicate that the electric field has a potential to alter the downward plasma flow at mid-latitudes during the magnetically quiet and disturbed periods investigated. Evidence was found that at the evening enhancement of the vertical upward $\boldsymbol{E} \times \boldsymbol{B}$ drift velocity, when the eastward electric field becomes increased before sunset, the mid-latitude ionosphere becomes depleted since the plasma flow from the plasmasphere to the ionosphere at mid-latitudes became reduced by the enhanced eastward electric field. Furthermore, the appearance of mid-latitude night-time TEC increases coincides with the event of vertical upward drift velocity reversal. It can be explained with the westward electric field, which triggers a downward plasma flow from the plasmasphere to the ionosphere at mid-latitudes. This plasma flow is the main source of plasma of these night-time TEC increases at mid-latitudes. Moreover, the conjugate mid-latitude night-time TEC increases are maintained during the operation of the reverse fountain, while the electric field is westward directed and while the downward plasma flow from the plasmasphere to the ionosphere at mid-latitudes continues. This paper also gave direct evidence that these low-and mid-latitude mechanisms associated with the east-west electric fields are not only substorm phenomena, as Park (1971) suggested, but also occur during magnetically quiet periods at high sunspot numbers.

Finally, it can be concluded that this paper gave a comprehensive demonstration – with a few, but well selected data sets – of the $\boldsymbol{E} \times \boldsymbol{B}$ drift velocity events, their resultant ionospheric features, their characteristic signatures, their effect on the low-latitude GPS recordings; and of the ionosphere-plasmasphere coupling. It also demonstrated how well the resultant ionospheric features can be observed with the different satellite techniques such as TOPEX and GPS, and what the practical consequences of these events are on the transionospheric signal propagation in the equatorial region. The good agreement found between the experimental observations obtained with the various different data sets of this paper and the published results of SUPIM (Balan and Bailey, 1995; Balan et al., 1997; Bailey et al., 1997) and Park (1971) was highlighted.

Acknowledgements. I. Horvath was supported by a La Trobe University Postgraduate Award (LUPA) and the Cooperative Research Centre for Satellite Systems (CRCSS). The authors thank the referees for their corrections and suggestions. Thanks are extended to AUSLIG and JPL for the satellite data, IPS for the ionosonde data, and Prof. K. Yumoto and Dr. Kazuo Shiokawa for the magnetic data. The TOPEX data were obtained from the NASA Physical Oceanography Distributed Active Archive Center at the Jet Propulsion Laboratory/California Institute of Technology.

Topical Editor M. Lester thanks two referees for their help in evaluating this paper.

References

Aarons, J., Mendillo, M., and Yantosca, R.: GPS phase fluctuations in the equatorial region during sunspot minimum, Radio Science 21, 347–350, 1997.

Appleton, E. V.: Two anomalies in the ionosphere, Nature 157, 691, 1946.

Bailey, G. J., Balan, N., and Su, Y. Z.: The Sheffield University plasmasphere ionosphere model - a review, J. Atmos. Terr. Phys., 59, 1541–1552, 1997.

Balan, N. and Bailey, G. J.: Equatorial plasma fountain and its effects: Possibility of an additional layer, J. Geophys. Res., 100, 21 421–21 432, 1995.

Balan, N., Bailey, G. J., Abdu, M. A., Oyama, K. I., Richards, P. G., MacDougall, J., and Batista, I. S.: Equatorial plasma fountain and its effects over three locations: Evidence for an additional layer, the F3-layer, J. Geophys. Res., 102, 2047–2056, 1997.

Blanc, M. and Richmond, A. D.: The ionospheric disturbance dynamo, J. Geophys. Res., 85, 1669–1686, 1980.

Chandra, H. and Rastogi, R. G.: Geomagnetic Storm Effects on Ionospheric Drifts and the Equatorial ES over the magnetic equator, Indian J. Radio Space Phys., 3, 332–336, 1974.

Fejer, B. G.: Equatorial ionospheric electric fields associated with magnetospheric disturbances, in: Solar wind-Magnetosphere coupling, (Eds) Kamide, Y. and Slavin, J. A., 519–545, Terra Scientific Publishing Company (TERRAPUB), Tokyo, 1986.

Fejer, B. G.: Low latitude electrodynamic drifts: a review, Journal of Atmospheric and Terrestrial Physics 53, 677–693, 1991.

Fejer, B. G., de Paula, E. R., Gonzales, S. A., and Woodman, R. F.: Average vertical and zonal F-region plasma drifts over Jicamarca, J. Geophys. Res., 96, 13 901–13 906, 1991.

Fejer, B. G. and Kelley, M. C.: Ionospheric irregularities, Rev. Geophys. Space Phys., 18, 401–454, 1980.

Johnson, J. L., Anderson, H. R., and Lagerloef, G. S. E.: Global ionosphere climatology from TOPEX/Poseidon, from http://www.nw.saic.com/tptec/, 1996.

Kelley, M. C.: The Earth's Ionosphere, Academic Press Inc., 1989.

Klobuchar, J. A.: Ionospheric effects on GPS, in: Global Positioning System: theory and applications, (Eds) Parkinson, B. W. and Spilker, J. J., Vol. 1, 485–515. Pub. American Institude of Aeronautics and Astronautics Inc., Washington, 1996.

Park, C. G.: Westward electric fields as the cause of nighttime enhancements in electron concentrations in mid latitude F-region, J. Geophys. Res., 76, 4560–4568, 1971.